

Synthetic Control of Kinetic Reaction Pathway and Cationic Ordering in High-Ni Layered Oxide Cathodes

Dawei Wang, Ronghui Kou, Yang Ren, Cheng-Jun Sun, Hu Zhao, Ming-Jian Zhang, Yan Li, Ashifia Huq, J. Y. Peter Ko, Feng Pan, Yang-Kook Sun, Yong Yang,* Khalil Amine,* Jianming Bai,* Zonghai Chen, and Feng Wang*

Nickel-rich layered transition metal oxides, $\text{LiNi}_{1-x}(\text{MnCo})_x\text{O}_2$ ($1-x \geq 0.5$), are appealing candidates for cathodes in next-generation lithium-ion batteries (LIBs) for electric vehicles and other large-scale applications, due to their high capacity and low cost. However, synthetic control of the structural ordering in such a complex quaternary system has been a great challenge, especially in the presence of high Ni content. Herein, synthesis reactions for preparing layered $\text{LiNi}_{0.7}\text{Mn}_{0.15}\text{Co}_{0.15}\text{O}_2$ (NMC71515) by solid-state methods are investigated through a combination of time-resolved in situ high-energy X-ray diffraction and absorption spectroscopy measurements. The real-time observation reveals a strong temperature dependence of the kinetics of cationic ordering in NMC71515 as a result of thermal-driven oxidation of transition metals and lithium/oxygen loss that concomitantly occur during heat treatment. Through synthetic control of the kinetic reaction pathway, a layered NMC71515 with low cationic disordering and a high reversible capacity is prepared in air. The findings may help to pave the way for designing high-Ni layered oxide cathodes for LIBs.

Lithium-ion batteries (LIBs) are preferred power sources for portable electronic devices and are increasingly being adopted for electric vehicles (EVs) and grid-level storage. However, large-scale application requires substantial improvement in energy density, cost, and lifetime of today's LIBs. Among them, energy density has been the largest hurdle to EV application, and so has aroused great research interest in developing new materials, especially cathodes, as they currently pose the main constrain to the energy density of the batteries. Layered transition metal oxides have been the dominant cathode materials for LIBs over decades, and among them, Ni-rich ones, $\text{LiNi}_{1-x}(\text{MnCo})_x\text{O}_2$ ($1-x \geq 0.5$), are the most promising candidates for their high specific capacity (180–220 mAh g⁻¹)^[1] compared

Dr. D. Wang, Dr. H. Zhao, Dr. M.-J. Zhang, Dr. F. Wang
Sustainable Energy Technologies Department
Brookhaven National Laboratory
Upton, NY 11973, USA
E-mail: fwang@bnl.gov

Dr. D. Wang, Prof. Y. Yang
Collaborative Innovation Center of Chemistry for Energy Materials
State Key Laboratory Physical Chemistry Solid Surfaces
Department of Chemistry
Xiamen University
Xiamen, Fujian 361005, China
E-mail: yyang@xmu.edu.cn

R. Kou, Dr. Y. Ren, Dr. C.-J. Sun
X-Ray Science Division
Advanced Photon Source
Argonne National Laboratory
Argonne, IL 60439, USA

Dr. M.-J. Zhang, Prof. F. Pan
School of Advanced Materials
Peking University Shenzhen Graduate School
Shenzhen, Guangdong 518055, P. R. China

Dr. Y. Li, Dr. K. Amine, Dr. Z. Chen
Chemical Sciences and Engineering Division
Argonne National Laboratory
Argonne, IL 60439, USA
E-mail: amine@anl.gov

Dr. A. Huq
Chemical and Engineering Materials Division
Oak Ridge National Laboratory
Oak Ridge, TN 37831, USA

Dr. J. Y. P. Ko
The Cornell High Energy Synchrotron Source
Cornell University, Ithaca
NY 14853, USA

Prof. Y.-K. Sun
Department of Energy Engineering
Hanyang University
Seoul 133-791, South Korea

Dr. J. Bai
National Synchrotron Light Source II
Brookhaven National Laboratory
Upton, NY 11973, USA
E-mail: jmbai@bnl.gov

 The ORCID identification number(s) for the author(s) of this article can be found under <https://doi.org/10.1002/adma.201606715>.

DOI: 10.1002/adma.201606715

to the commercially available cathodes, such as LiCoO_2 (140 mAh g^{-1}), LiFePO_4 (170 mAh g^{-1}), and $\text{LiNi}_{1/3}\text{Co}_{1/3}\text{Mn}_{1/3}\text{O}_2$ (160 mAh g^{-1}).^[2] In addition, the cost of these materials would be reduced with the reduction of cobalt content.

In order to further boost Li storage capacity, research efforts are now increasingly focused on developing $\text{LiNi}_{1-x}(\text{MnCo})_x\text{O}_2$ with even higher Ni content, i.e., $1-x \geq 0.7$. However, cycling stability and safety are often compromised as a result of high Ni reactivity and structural reconstruction on the particle surface.^[3] On the other hand, structural disordering as a result of cationic mixing in octahedral sites becomes an issue when Ni content increases to high values.^[4] Therein, the cationic mixing originates from the propensity of Ni to form Ni^{2+} and the low energy barrier for the migration of Ni^{2+} ions,^[5] leading to a detrimental effect on Li diffusivity, cycling stability, first-cycle efficiency, and overall electrode performance.^[6] Over the years, significant efforts have been dedicated to improving the electrochemical performance of Ni-rich layered oxide cathodes via reduction of cationic mixing and tuning surface chemistry through various approaches, such as lattice doping,^[7] composition tuning,^[8] surface modification,^[9] and special design of core-shell and/or concentration gradient structures.^[10] Although surface or bulk modifications are important for improving the electrochemical performance of electrodes, implementation of these strategies to make materials of desired structure and properties was often found difficult due to the complexity of the synthesis reactions, especially for such a complex quaternary system, $\text{LiNi}_{1-x}(\text{MnCo})_x\text{O}_2$, wherein the ordering of multiple cations (Ni, Co, and Mn, in addition to Li ions) within a cubic close packed O-anion framework is involved. As a result, precise control of the cationic ordering via tuning the thermodynamic and kinetic conditions during synthesis is critical to making desired phases and material properties, especially in the presence of high Ni content (i.e., $1-x \geq 0.7$).

In situ X-ray diffraction (XRD) has been shown to be a powerful tool capable of probing electrochemical reactions of battery electrodes, and has also been applied to tracking synthesis reactions in preparing battery materials under real synthesis conditions.^[11] In recent efforts, in situ XRD measurements have been applied to studies of phase transitions in intermediates during solid-state synthesis of Ni-rich layered oxide cathodes.^[12] These in situ studies not only provided details of phase evolution, from precursors to intermediates, and to the layered phase during heat treatment, but also revealed a direct correlation of synthesis conditions to Li and transition metal (TM) slab distances, thereby to their electrochemical properties. Following the previous studies on synthesis of LiNiO_2 , $\text{LiNi}_{0.8}\text{Co}_{0.2}\text{O}_2$, and $\text{LiNi}_{0.6}\text{Mn}_{0.2}\text{Co}_{0.2}\text{O}_2$,^[12] in situ studies were further conducted on synthesis reactions in preparing high-Ni layered $\text{LiNi}_{0.7}\text{Mn}_{0.15}\text{Co}_{0.15}\text{O}_2$ (NMC71515) under ambient atmosphere for insights into synthetic control of structural ordering in the material. In this study, time-resolved in situ high-energy XRD (HEXRD) and X-ray absorption spectroscopy (XAS) were employed, coupled with quantitative data analysis, to track the kinetic reaction pathway and cationic ordering in the intermediates toward forming NMC71515 when subjected to heat treatment at three different temperatures (800, 850, and 900 °C). The real-time observation revealed a dynamically competing cationic ordering/disordering process, arising from thermal-driven cationic oxidation and lithium/oxygen loss in NMC71515 that

concomitantly occurs during heat treatment. Through synthetic control of kinetic reaction pathway, the structural ordering of the final products was tuned for obtaining highly-ordered NMC71515 with excellent electrochemical performance, even in air. The findings shed light on designing high-performance high-Ni layered oxides through synthetic control of the kinetic reaction pathway and structural ordering in the materials.

Figure 1a shows the time-resolved in situ HEXRD patterns recorded from intermediates of NMC71515 during heat treatment at 850 °C in air; similar measurements were also made at 800 and 900 °C, and the results are given in Figures S1 and S2 (Supporting Information). The layered structure was already formed in the materials at the target temperatures, since they had been preheated at 500 °C, and the extension of holding time led to improvement of structural ordering, as indicated by the continuous increase of peak intensity in (003) and (104) reflections, and enlarged splitting of (018)/(110) peaks (Figure 1c–e). Meanwhile, these peaks became narrower, indicating the enhancement of crystallinity of the materials during heat treatment. In contrast to the slow increase of integrated intensity of (104) peak, the integrated intensity of the (003) peak increased quickly as a result of cationic ordering (Figure 1b), which will be further discussed below based on quantitative structure analysis. A similar variation trend was observed in the intermediates heated at 800 and 900 °C (Figures S1 and S2, Supporting Information), except that a small amount of residual Li_2CO_3 existed throughout the heat treatment at 800 °C (Figures S1a and S5, Supporting Information).

The evolution of the oxidation states of TMs in NMC71515 (namely, Ni, Mn, and Co) were tracked by time-resolved in situ XAS (Figure 1f and Figure S3 (Supporting Information)), for correlation with structural evolution. During the preheating process, oxidation to TMs had already occurred, bringing Co and Mn to the highest oxidation states (i.e., Co^{3+} and Mn^{4+} ; indicated by no variation of their K-edge near-edge spectra as in Figure S3 in the Supporting Information), and slight edge shift to higher energies was observed in Ni K-edge during heat treatment at 850 °C (Figure 1f). The results are consistent with the in situ HEXRD observation (Figure 1), indicating that a layered structure was formed in NMC71515 upon reaching 850 °C, and heat treatment at the same temperature led to further oxidation of Ni and structural ordering in the material. In addition, the overall morphology of secondary particles, with a size of around 10 μm (shown by scanning electron microscopy (SEM) images in Figure 1g), was maintained throughout the heat treatment process (as to be discussed below).

In order to identify subtle structural changes in the involved intermediates toward layered NMC71515 during heat treatment, Rietveld refinement was performed on individual HEXRD patterns obtained from in situ measurements. Different structure models, spinel ($Fd\bar{3}m$), layered ($R\bar{3}m$), and hybrid spinel/layered, were tried for refining the patterns of preheated samples, showing that refinement based on the layered model provided the best fitting to the diffraction patterns (as discussed in Figure S4 in the Supporting Information). In order to identify the local environment of Li in the layered structure, high-resolution ^6Li nuclear magnetic resonance (NMR) spectra were measured from the samples preheated at 500 °C and after heat treatment at 800 °C. The main results are given in Figure S5 (Supporting Information). In the ^6Li NMR spectra

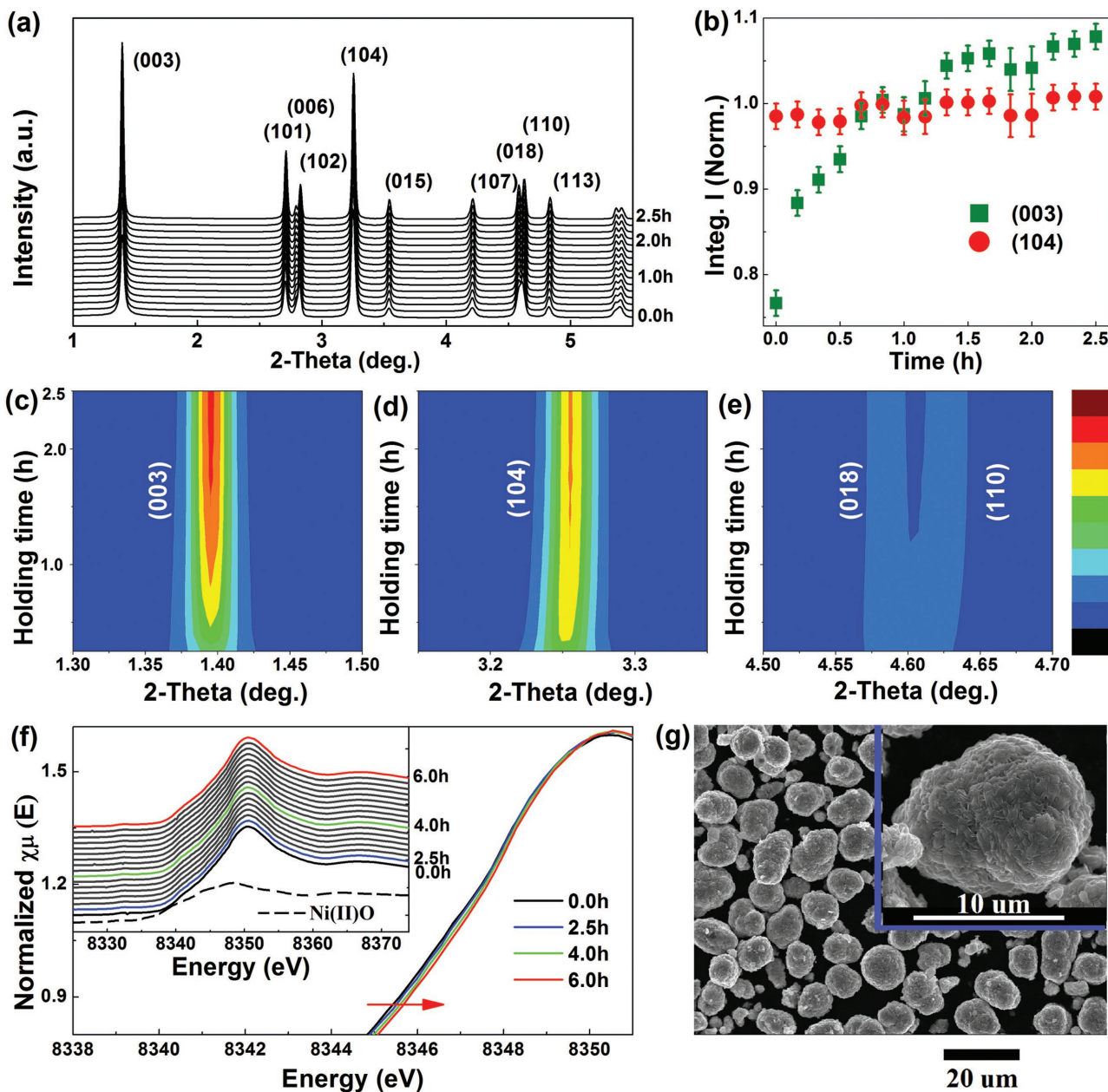


Figure 1. In situ tracking of the structural evolution of the intermediates during solid-state synthesis of $\text{LiNi}_{0.7}\text{Mn}_{0.15}\text{Co}_{0.15}\text{O}_2$ (NMC71515) at $850\text{ }^\circ\text{C}$ in the air (see also Figures S1 and S2 in the Supporting Information for the results from similar measurements carried out at $800\text{ }^\circ\text{C}$ and $900\text{ }^\circ\text{C}$). a) Time-resolved high-energy X-ray diffraction patterns. b) Evolution of the integrated intensity of the (003) and (104) reflections during heat treatment. c–e) Intensity maps for the characteristic reflections of layered structure, (003), (104), (018), and (110), indicating gradual improvement of structural ordering with time. f) Time-resolved X-ray absorption near-edge spectra of Ni K-edge (inset), and a zoom-in view of selected spectra obtained at 0 h (black), 2.5 h (blue), 4 h (green), and 6 h (red); slight chemical shift to higher energies is illustrated by a red arrow. g) Scanning electron microscopy image of particles after preheat treatment at $500\text{ }^\circ\text{C}$.

for the preheated sample, three peaks at about 0, 550, and 1200 ppm were observed and can be attributed to Li from residual Li_2CO_3 , at 3b sites, at 3a antisites, respectively.^[13] Compared to the preheated samples, the residual of Li_2CO_3 in the sample heated at $800\text{ }^\circ\text{C}$ is much reduced, and correspondingly the signal from Li at 3a antisites became very weak and is barely detectable by NMR. Therefore, a cationic mixing model with both Li and Ni occupying antisites, namely

$(\text{Li}_{1-x}\text{Ni}_x)_{3b}(\text{Ni}_{0.7-0.3x-0.7y}\text{Co}_{0.15+0.15x-0.15y}\text{Mn}_{0.15+0.15x-0.15y}\text{Li}_y)_{3a}\text{O}_2$ was used to refine all sets of in situ HEXRD data.^[14] Some more details of the refinement are given in the Experimental Section (Supporting Information), and the main results from refinement are provided in Figure 2 and Figure S6 and Table S1 (Supporting Information).

As shown in Figure 2a, the occupancy of Ni^{2+} ions at 3b (Li sites) decreased exponentially during heat treatment at the

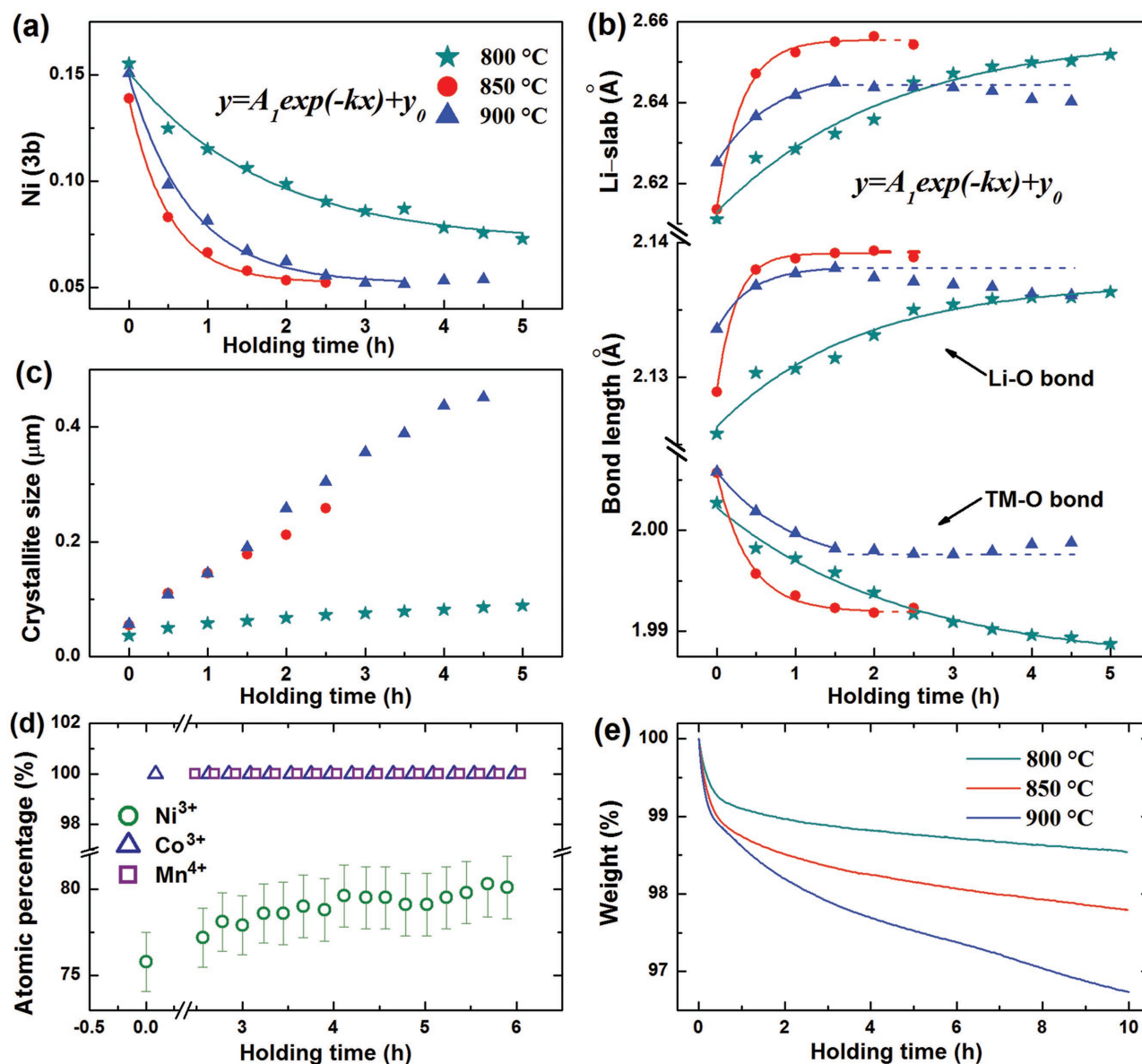


Figure 2. Structural ordering in NMC71515 during heat treatment at constant temperatures: 800 °C (dark cyan), 850 °C (red), 900 °C (blue). a) Evolution of the cationic disordering (i.e., occupancy of Ni ions at 3b sites). b) Variation of Li-slab distance (top), and bond length of Li–O and TM–O (bottom). Solid lines are the fitting results based on exponential equation ($y = A_1 \exp(-kx) + y_0$), dashed lines are the extrapolations of the fits. c) Evolution of crystallite size. d) Evolution of the atomic percentage of Ni^{3+} , Co^{3+} , and Mn^{4+} (determined from the in situ X-ray absorption spectroscopy data in Figure 1f and Figure S3 in the Supporting Information). e) Thermogravimetric analysis curves of the preheated precursors subjected to further heat treatment.

three different temperatures (i.e., 800, 850, and 900 °C). As a consequence, lattice parameter a decreased, while c increased (in the early stages), leading to a fast increase of c/a value during holding at 800 and 850 °C (Figure S6a,b, Supporting Information). During holding at 900 °C, evolution of lattice parameter a showed a parabolic behavior with open upward, while lattice parameter c kept increasing (especially at the early stage), leading to a parabolic shape of c/a that opens downward, with the maximum reached at about 3.5 h (Figure S6a–c, Supporting Information). As expected, more Ni ions moved to 3a sites (Figure S6d, Supporting Information), and the occupancy of Co and Mn at 3a sites relatively decreased, in a very small amplitude, during

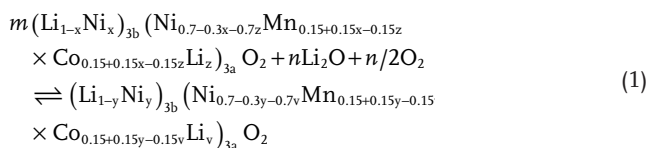
the entire holding process (Figure S6e, Supporting Information). At higher temperatures (i.e., 850 and 900 °C), occupancy of Ni at 3b sites reached a minimum quickly, and thereafter moved reversely, showing a parabolic shape with open upward. However, changes at 800 °C occurred at a much slower pace, and did not reach a minimum within the experimental time.

A similar trend was found in the evolution of Li–O, TM–O bond lengths and Li-slab, TM-slab distances (as shown in Figure 2b and Figure S6f (Supporting Information)), namely showing a parabolic behavior with open downward or upward with time, at 850 and 900 °C, while those evolutions occurred at a slower rate at 800 °C. During holding process, crystallite

size increased almost linearly with time at the three different temperatures, 800, 850, and 900 °C, to about 0.1, 0.26, and 0.45 μm, respectively, in the final products (Figure 2c). The results from refinement are overall consistent with SEM observations (Figure S7, Supporting Information), showing that the large ≈10 μm sized secondary particles were maintained (as compared to the preheated samples; Figure 1g).

Bicomponent linear fitting was performed to the X-ray near-edge spectra (XANES) of the Co, Mn, and Ni K-edges (as given in Figure 1f and Figures S3 and S8 (Supporting Information)). The main results were given in Figure 2d (see also Figure S8 and Table S2 in the Supporting Information for the details of the fitting process), showing that the fraction of Mn⁴⁺, Co³⁺ kept unity, while that of Ni³⁺ increased slowly with time during holding. So, the combination of in situ XAS and HEXRD observations indicates a gradual oxidation of Ni²⁺ and migration from 3b to 3a sites, thereby leading to improvement of cationic ordering in the material during the heat treatment.

The overall reaction of intermediate phases is believed to follow the process^[14]



Where $m = (1 + y)/(1 + x)$ and $n = (x - y)/(1 + x)$ for $x > y$. The forward reaction represents the cationic ordering process and the reverse reaction represents the cationic disordering (namely Li/Ni mixing) process, which is caused by the propensity of Ni to form Ni²⁺ in face-centered cubic octahedral sites and lithium loss at high temperatures.^[15]

The results from quantitative structural analysis (as shown in Figure 2 and Figure S6 in the Supporting Information) indicate strong time dependence of structure parameters, such as occupancy of TM ions at 3a, 3b sites, Li–O, TM–O bond lengths, and Li-slab, TM-slab distances, which are directly correlated to the degree of structural ordering. So, the evolution of these structural parameters was used to evaluate kinetics of the ordering reaction by fitting the data to an exponential equation ($y = A_1 \exp(-kx) + y_0$), where k is defined as the coefficient of the ordering reaction. The fitting results are listed in Table S3 (Supporting Information). Throughout the synthesis process at 800 °C data followed the exponential profiles very well, indicating slow lithium loss, and further increase of holding time lead to gradual improvement of the ordering. However, low crystallite growth rate and existence of residual Li₂CO₃ suggested that 800 °C may not be high enough to get a well-ordered phase within limited time. Similarly, at the beginning of synthesis process at 850 °C, parameters of the Ni occupancies, bond lengths, and slab distances followed the exponential profile well. After 2 h, deviation from exponential profiles was observed, indicating serious Li loss, and consequently breaking of the equilibrium. A similar trend was found during heat treatment at 900 °C, after holding for 1.5 h, data began to deviate from the exponential profiles, and such an accelerated deviation may be due to quick Li/O loss at such high temperature, as indicated by thermogravimetric analysis (Figure 2e). Interestingly,

in contrast to the accelerated Li/O loss with an elevation of temperature, the highest speed of structural ordering was achieved at 850 °C, indicated by the time dependence of structure parameters, such as occupancy of TMs at 3a, 3b sites, Li–O, TM–O bond lengths, and Li-slab, TM-slab distances (Figure 2a,b).

Thermodynamically, the forward Li/Ni ordering process should have a lower activation energy (E_a) than that of the reverse Li/Ni mixing process (E_a'), namely $E_a < E_a'$, which means the Li/Ni mixing process is more responsive to temperature according to the Arrhenius relationship, $k = k_0 \exp\left(-\frac{E_a}{KT}\right)$.^[5d]

Although elevation of heating temperature will lead to an increase in the reaction coefficient and reaction rates for both the forward reaction and reverse reaction, the increase of reaction coefficient of the reverse reaction should be larger than that of forward reaction because of its higher activation energy. Therefore, the overall reaction rate should be temperature dependent $v = k_1 c_1 - k_2 c_2$, and reach the maximum

at $\frac{dk_1}{dT} c_1 = \frac{dk_2}{dT} c_2$, as do the apparent coefficient (k_{app}). Here,

c_1 and c_2 are the concentration of reactants and products. The enthalpy difference between the forward process and backward process of the overall reaction $H = E_a - E_a' < 0$. The entropy difference S between the final phase and the intermediates should be negative because it is an ordering process. Therefore, the difference of Gibbs free energy between the forward process and backward, G ($G = H - TS$), should be temperature dependent, and higher heating temperature would lead to a larger G , which will push the final pseudoequilibrium K backward because of $G = -RT \ln K$. In addition, the serious lithium loss at higher temperature will further push the reaction backward, thus leading to a shortened time of reaching the maximum or minimum points with an increase of heating temperature. In short, from the view of thermodynamics, a lower heating temperature and longer holding time are beneficial to the ordering of final products once the temperature is high enough to provide necessary activation energy (E_a) for the ordering. However, because of the Li/O loss under real synthesis conditions, thermodynamics and kinetics should be balanced via tuning heating temperature and holding time, which has been revealed by this in situ study.

The largest ordering coefficient was observed at about 850 °C (in Figure 2a,b and Table S3 in the Supporting Information), and heat treatment at the temperature for 2.5 h leads to the reduction of Ni²⁺ on 3b sites to about 5.2%. The value was further reduced to 4.1% after cooling down to room temperature, indicating that cationic ordering also happened during the cooling process. With data from in situ measurements, the lowest Li⁺/Ni²⁺ mixing, the largest Li bond length and Li-slab distance, were obtained in the samples heated at 850 °C. The trend of changes in Li-slab distance and cationic mixing is consistent with the predication by first principle calculations, in that the cationic mixing should cause reduction of Li-slab distance.^[6a] Importantly, a slight reduction in Li-slab distance (4%) may cause a great increase in activation energy (more than 200%) or a few orders of magnitude reduction in lithium diffusivity.^[6a,12b] Therefore, in order to obtain high electrochemical activity, control of the Li-slab distance of the layered oxides is needed and may be realized via fine-tuning of the synthesis conditions (temperature in particular).

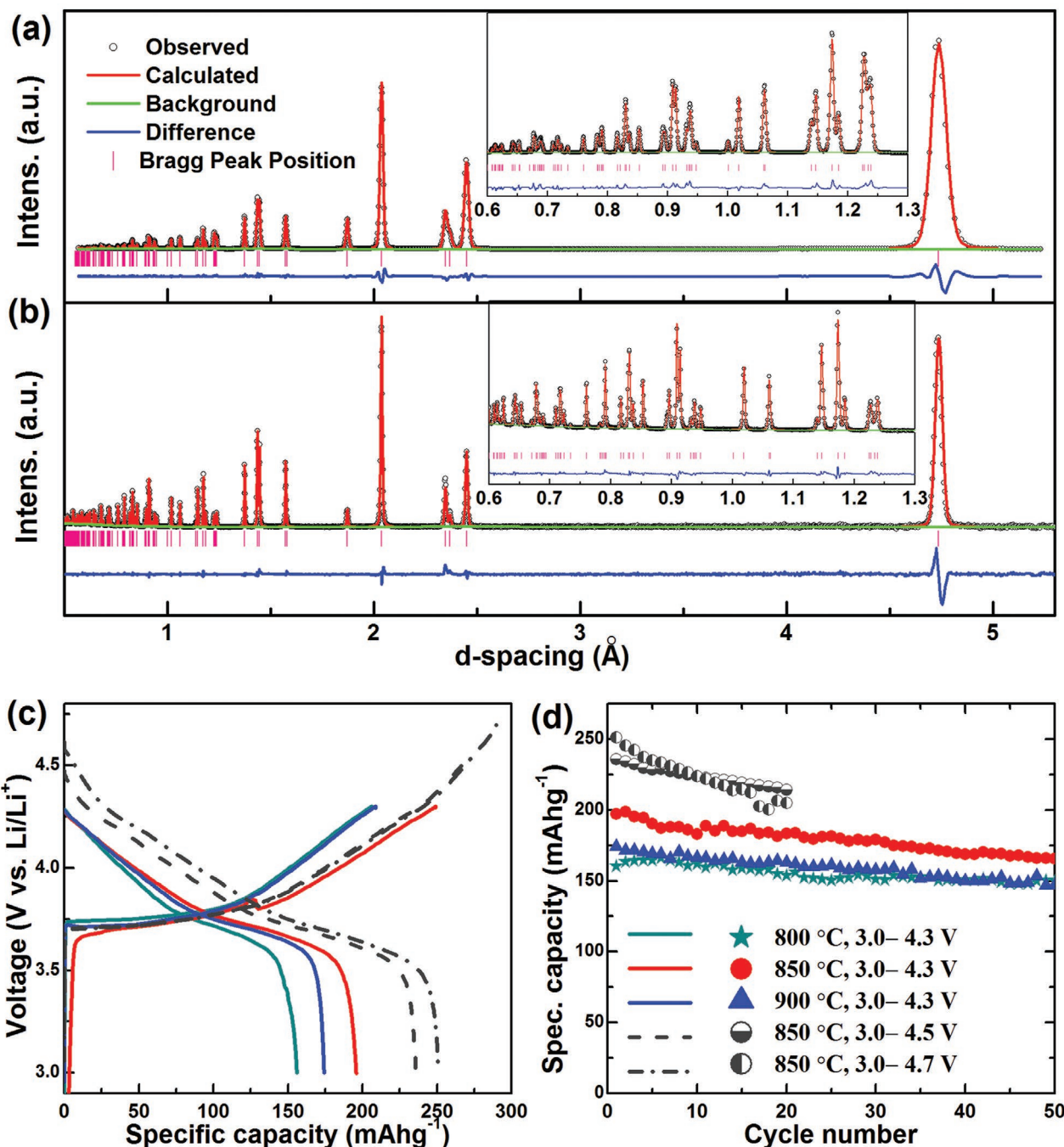


Figure 3. Structural and electrochemical properties of NMC71515 synthesized at different temperatures (800, 850, 900 °C). a,b) Synchrotron X-ray and neutron diffraction patterns of NMC71515 after heat treatment at 850 °C for 5 h (see also Figure S9 in the Supporting Information for the samples obtained at 800, 900 °C). The enlarged spectra in small d spacing range are shown in the inset. In the plots, open circles are used for the observed data, red lines for the calculated data, pink bars for Bragg positions, blue lines for the difference between the observed and calculated data, and green lines for the refined background. c,d) Charge/discharge voltage profiles, and the corresponding cycling performance of NMC71515 synthesized at 800 °C (dark cyan), 850 °C (red), 900 °C (blue). A constant current of 10 mA g⁻¹ and voltage window of 3.0–4.3 V were used for most of the electrochemical tests. Tests were also made in wider voltage windows, 3.0–4.5 V (gray dashed line) and 3.0–4.7 V (gray dashed-dotted line) for the sample obtained at 850 °C, demonstrating achievable higher capacity in the extended voltage range.

Following similar procedures as performed for in situ studies, NMC71515 powder was synthesized at 800, 850, and 900 °C for 5 h and examined using high-resolution XRD and neutron powder diffraction (NPD). The XRD patterns of

the final products are presented in **Figure 3a** and **Figure S9** (Supporting Information). These sets of data were refined using the same layered model (as done for the in situ data), yielding the values of Li/Ni mixing: 3.2%, 2.6%, and 4.4% for

samples heated at 800, 850, and 900 °C, respectively (Table S4, Supporting Information). The results are overall consistent with in situ experiments, both indicating that 850 °C should be the most suitable heating temperature. The NPD pattern of NMC71515 heated at 850 °C, along with the refinement, was given in Figure 3b, indicating 2.8% of Ni occupied at 3b sites, which matched well with the XRD data. A small difference in Li/Ni mixing between the in situ and ex situ data might be due to different cooling process between the two measurements.

Electrochemical tests were also made on NMC71515 by making electrodes from powder synthesized at three different temperatures (800, 850, and 900 °C). Figure 3c shows the charge–discharge profiles, indicating much higher initial discharge capacity in the samples synthesized at 850 °C (with the value of 197 mAh g⁻¹), compared to that obtained at 800 and 900 °C (162 and 174 mAh g⁻¹, respectively). In addition, lower overpotential was obtained in the sample heated at 850 °C (Figure 3c). The electrochemical performance is in good agreement with structural analysis, that is, the sample heated at 850 °C has the lowest Li/Ni mixing at 3b sites, the largest Li slab, and moderate crystallite size. In addition, excellent capacity retentions were obtained in the three samples heated at 800, 850, and 900 °C, of 93.5%, 84.1%, and 84.5% after 50 cycles (Figure 3d). The extension of electrochemical windows to 4.5, 4.7 V led to greatly increased discharge capacity, but at the cost of capacity retention (Figure 3c,d), possibly due to the side reaction on the surface and structure degradation upon overcharge.^[3]

In summary, time-resolved in situ HEXRD and XAS studies were conducted on synthesis reactions in preparing NMC71515 under ambient atmosphere. The results from quantitative structure analysis showed complex cationic ordering and disordering processes that concurrently occur throughout the heat treatment process. Temperature was shown to be crucial to the kinetics of cationic ordering and the highest ordering coefficient was obtained at 850 °C during the heat treatment of NMC71515 in the air. Guided by insights from in situ studies, we were able to synthesize NMC71515 with low Li⁺/Ni²⁺ mixing, large Li slab, and moderate crystallite size, which exhibited high capacity (up to 200 mAh g⁻¹) and excellent retention. The method developed in this study may open a new avenue for kinetic control of the reaction pathway and cationic ordering during synthesis of layered oxides, thereby obtaining the materials with desired structural/electrochemical properties.

Supporting Information

Supporting Information is available from the Wiley Online Library or from the author.

Acknowledgements

This work was supported by the U.S. Department of Energy (DOE) Office of Energy Efficiency and Renewable Energy under the Advanced Battery Materials Research (BMR) program, Contract No. DE-SC0012704. SEM measurements carried out at the Center for Functional Nanomaterials, Brookhaven National Laboratory, were supported by the U.S. Department of Energy, Office of Basic Energy Sciences, under Contract

No. DE-SC0012704. Sector 20 facilities at the Advanced Photon Source, and research at these facilities, are supported by the US Department of Energy – Basic Energy Sciences, the Canadian Light Source and its funding partners, and the Advanced Photon Source. Use of the Advanced Photon Source, an Office of Science User Facility operated for the U.S. Department of Energy (DOE) Office of Science by the Argonne National Laboratory is operated for the U.S. Department of Energy by Chicago Argonne, LLC, under contract DE-AC02-06CH11357. Y.Y. would like to acknowledge the National Natural Science Foundation of China (Grant Nos. 21233004, 21473148, 21428303, 21621091) for their research. J.B. would like to acknowledge support of the NSLS-II, a U.S. Department of Energy (DOE) Office of Science User Facility operated for the DOE Office of Science by the Brookhaven National Laboratory, under Contract No. DE-SC0012704. Neutron powder diffraction measurement at ORNL's Spallation Neutron Source, was sponsored by the Scientific User Facilities Division, Office of Basic Energy Sciences, US Department of Energy. SEM measurements carried out at the Center for Functional Nanomaterials, Brookhaven National Laboratory, were supported by the U.S. Department of Energy, Office of Basic Energy Sciences, under Contract No. DE-SC0012704. The synchrotron XRD work conducted at the Cornell High Energy Synchrotron Source (CHESS) was supported by the National Science Foundation under award DMR-1332208. This work was also supported by the Global Frontier R&D Program (2013M3A6B1078875) on Center for Hybrid Interface Materials (HIM) funded by the Ministry of Science, Information & Communication Technology (ICT) and the Human Resources Development program (No. 20154010200840) of the Korea Institute of Energy Technology Evaluation and Planning (KETEP) grant funded by the Korea government Ministry of Trade, Industry and Energy.

Conflict of Interest

The authors declare no conflict of interest.

Keywords

cationic ordering, high-energy X-ray diffraction, layered oxide cathodes, lithium-ion batteries, X-ray absorption spectroscopy

Received: December 13, 2016

Revised: April 1, 2017

Published online:

- [1] a) S. K. Jung, H. Gwon, J. Hong, K. Y. Park, D. H. Seo, H. Kim, J. Hyun, W. Yang, K. Kang, *Adv. Energy Mater.* **2014**, *4*, 1300787; b) Z. Wu, S. Ji, J. Zheng, Z. Hu, S. Xiao, Y. Wei, Z. Zhuo, Y. Lin, W. Yang, K. Amine, F. Pan, *Nano Lett.* **2015**, *15*, 5590; c) B. B. Lim, S. J. Yoon, K. J. Park, C. S. Yoon, S. J. Kim, J. J. Lee, Y.-K. Sun, *Adv. Funct. Mater.* **2015**, *25*, 4673; d) S.-T. Myung, H.-J. Noh, S.-J. Yoon, E.-J. Lee, Y.-K. Sun, *J. Phys. Chem. Lett.* **2014**, *5*, 671; e) J. Lu, Z. Chen, Z. Ma, F. Pan, L. A. Curtiss, K. Amine, *Nat. Nanotechnol.* **2016**, *11*, 1031.
- [2] a) M. S. Whittingham, *Chem. Rev.* **2014**, *114*, 11414; b) A. Manthiram, J. C. Knight, S. T. Myung, S. M. Oh, Y.-K. Sun, *Adv. Energy Mater.* **2016**, *6*, 1501010.
- [3] F. Lin, I. M. Markus, D. Nordlund, T.-C. Weng, M. D. Asta, H. L. Xin, M. M. Doeff, *Nat. Commun.* **2014**, *5*, 3529.
- [4] a) W. Liu, P. Oh, X. Liu, M. J. Lee, W. Cho, S. Chae, Y. Kim, J. Cho, *Angew. Chem. Int. Ed.* **2015**, *54*, 4440; b) P. Rozier, J. M. Tarason, *J. Electrochem. Soc.* **2015**, *162*, A2490; c) A. Manthiram, B. Song, W. Li, *Energy Storage Mater.* **2017**, *6*, 125.
- [5] a) A. Van der Ven, G. Ceder, *Electrochem. Solid-State Lett.* **2000**, *3*, 301; b) J. Reed, G. Ceder, *Electrochem. Solid-State Lett.* **2002**, *5*,

- A145; c) J. Reed, G. Ceder, *Chem. Rev.* **2004**, *104*, 4513; d) Y. Kim, D. Kim, S. Kang, *Chem. Mater.* **2011**, *23*, 5388.
- [6] a) K. Kang, G. Ceder, *Phys. Rev. B* **2006**, *74*, 094105; b) J. Lee, A. Urban, X. Li, D. Su, G. Hautier, G. Ceder, *Science* **2014**, *343*, 519; c) S. Zheng, R. Huang, Y. Makimura, Y. Ukyo, C. A. Fisher, T. Hirayama, Y. Ikuhara, *J. Electrochem. Soc.* **2011**, *158*, A357; d) S. Cui, Y. Wei, T. Liu, W. Deng, Z. Hu, Y. Su, H. Li, M. Li, H. Guo, Y. Duan, W. Wang, M. Rao, J. Zheng, X. Wang, F. Pan, *Adv. Energy Mater.* **2016**, *6*, 1501309.
- [7] a) S.-U. Woo, B.-C. Park, C. Yoon, S.-T. Myung, J. Prakash, Y.-K. Sun, *J. Electrochem. Soc.* **2007**, *154*, A649; b) S.-W. Woo, S.-T. Myung, H. Bang, D.-W. Kim, Y.-K. Sun, *Electrochim. Acta* **2009**, *54*, 3851.
- [8] a) K.-S. Lee, S.-T. Myung, K. Amine, H. Yashiro, Y.-K. Sun, *J. Electrochem. Soc.* **2007**, *154*, A971; b) H.-G. Kim, S.-T. Myung, J. K. Lee, Y.-K. Sun, *J. Power Sources* **2011**, *196*, 6710; c) J. Zheng, W. H. Kan, A. Manthiram, *ACS Appl. Mater. Interfaces* **2015**, *7*, 6926.
- [9] a) Y. Chen, Y. Zhang, B. Chen, Z. Wang, C. Lu, *J. Power Sources* **2014**, *256*, 20; b) Y. Huang, F.-M. Jin, F.-J. Chen, L. Chen, *J. Power Sources* **2014**, *256*, 1; c) Z. Wu, S. Ji, T. Liu, Y. Duan, S. Xiao, Y. Lin, K. Xu, F. Pan, *Nano Lett.* **2016**, *16*, 6357.
- [10] a) Y.-K. Sun, Z. Chen, H.-J. Noh, D.-J. Lee, H.-G. Jung, Y. Ren, S. Wang, C. S. Yoon, S.-T. Myung, K. Amine, *Nat. Mater.* **2012**, *11*, 942; b) Y.-K. Sun, S.-T. Myung, B.-C. Park, J. Prakash, I. Belharouak, K. Amine, *Nat. Mater.* **2009**, *8*, 320; c) S.-J. Yoon, K.-J. Park, B.-B. Lim, C. S. Yoon, Y.-K. Sun, *J. Electrochem. Soc.* **2015**, *162*, A3059; d) H.-J. Noh, S.-T. Myung, Y. J. Lee, Y.-K. Sun, *Chem. Mater.* **2014**, *26*, 5973; e) Y.-K. Sun, S.-T. Myung, M.-H. Kim, J. Prakash, K. Amine, *J. Am. Chem. Soc.* **2005**, *127*, 13411.
- [11] a) K. W. Nam, S. M. Bak, E. Hu, X. Yu, Y. Zhou, X. Wang, L. Wu, Y. Zhu, K. Y. Chung, X. Q. Yang, *Adv. Funct. Mater.* **2013**, *23*, 1047; b) X.-J. Wang, H.-Y. Chen, X. Yu, L. Wu, K.-W. Nam, J. Bai, H. Li, X. Huang, X.-Q. Yang, *Chem. Commun.* **2011**, *47*, 7170; c) X. Yu, H. Pan, W. Wan, C. Ma, J. Bai, Q. Meng, S. N. Ehrlich, Y.-S. Hu, X.-Q. Yang, *Nano Lett.* **2013**, *13*, 4721; d) J. Bai, J. Hong, H. Chen, J. Graetz, F. Wang, *J. Phys. Chem. C* **2015**, *119*, 2266; e) G.-L. Xu, Z. Chen, G.-M. Zhong, Y. Liu, Y. Yang, T. Ma, Y. Ren, X. Zuo, X.-H. Wu, X. Zhang, K. Amine, *Nano Lett.* **2016**, *16*, 3955; f) Z. Chen, Y. Ren, Y. Qin, H. Wu, S. Ma, J. Ren, X. He, Y.-K. Sun, K. Amine, *J. Mater. Chem.* **2011**, *21*, 5604; g) M. P. Glazer, J. S. Okasinski, J. D. Almer, Y. Ren, *MRS Bull.* **2016**, *41*, 460; h) F. Wang, L. Wu, B. Key, X. Q. Yang, C. P. Grey, Y. Zhu, J. Graetz, *Adv. Energy Mater.* **2013**, *3*, 1324.
- [12] a) Y. Li, R. Xu, Y. Ren, J. Lu, H. Wu, L. Wang, D. J. Miller, Y.-K. Sun, K. Amine, Z. Chen, *Nano Energy* **2016**, *19*, 522; b) J. Zhao, W. Zhang, A. Huq, S. T. Mixture, B. Zhang, S. Guo, L. Wu, Y. Zhu, Z. Chen, K. Amine, F. Pan, J. Bai, F. Wang, *Adv. Energy Mater.* **2016**, *7*, 1601266.
- [13] W.-S. Yoon, S. Iannopollo, C. P. Gley, D. Carlier, J. Gorman, J. Reed, G. Ceder, *Electrochem. Solid-State Lett.* **2004**, *7*, A167.
- [14] A. Rougier, I. Saadoun, P. Gravereau, P. Willmann, C. Delmas, *Solid State Ionics* **1996**, *90*, 83.
- [15] H. H. Li, N. Yabuuchi, Y. S. Meng, S. Kumar, J. Breger, C. P. Grey, Y. Shao-Horn, *Chem. Mater.* **2007**, *19*, 2551.